Journal of Neuroscience Methods 131 (2003) 195–203

JOURNAL OF NEUROSCIENCE METHODS

www.elsevier.com/locate/jneumeth

Analyzing the reflections from single ommatidia in the butterfly compound eye with Voronoi diagrams

Kurt J.A. Vanhoutte [a,*], Kristel F.L. Michielsen [b], Doekele G. Stavenga [a]

[a] *Department of Neurobiophysics, University of Groningen, Nijenborgh 4, 9747 AG Groningen, The Netherlands*
[b] *Department of Applied Physics and Materials Science Centre, University of Groningen, Nijenborgh 4, 9747 AG Groningen, The Netherlands*

Received 4 June 2003; received in revised form 23 August 2003; accepted 26 August 2003

Abstract

This paper presents a robust method for the automated segmentation and quantitative measurement of reflections from single ommatidia in the butterfly compound eye. Digital pictures of the butterfly eye shine recorded with a digital camera are processed to yield binary images from which single facet centers can be extracted using a morphological image analysis procedure. The location of the facet centers is corrected by fitting in-line facet centers to a second-order polynomial. Based on the new centers a Voronoi diagram is constructed. In the case of the eye shine images, the Voronoi diagram defines a hexagonal lattice that overlaps with the original facet borders, allowing instantaneous quantification of the reflections from single ommatidia. We provide two typical examples to demonstrate that the developed technique may be a powerful tool to characterize in vivo the heterogeneity of butterfly eyes and to study the dynamic control of the light flux by the pupil mechanism.

Keywords: Butterfly ommatidia; Eye shine; Image analysis; Pupil mechanism; Eye heterogeneity

1. Introduction

Observing butterfly eyes with an epi-illumination microscope reveals an often spectacular eye shine, which is due to the reflection of incident light on a multilayer tapetum, created in each ommatidium by tracheoles proximal of the light-guiding rhabdom (Miller and Bernard, 1968). The eye shine phenomenon is highly useful for non-invasive, optical investigations of retinal processes, e.g. the photochemistry of visual pigments (Bernard, 1979; Bernard and Remington, 1991; Stavenga, 1975; Stavenga, 1979) and the light-dependence and dynamics of the pupil mechanism (Järemo Jonson et al., 1998; Stavenga et al., 1977). The eye shine is especially bright when observed with the microscope focused at the level of the center of curvature of the eye, because of the approximately spherical shape of compound eyes and the appearance there of the so-called deep pseudopupil (Franceschini and Kirschfeld, 1971). The deep pseudopupil is the superimposed image of numerous rhabdoms projected by the corresponding dioptrical systems, and therefore measurements on the deep pseudopupil have an optimal signal-to-noise ratio. However, because of the superposition, the obtained signal is an average of several ommatidia. Recent research has demonstrated that the ommatidia of butterfly eyes can be highly heterogeneous (Arikawa and Stavenga, 1997; Stavenga, 2002a,b), and this heterogeneity is obscured in deep pseudopupil measurements. This paper presents a novel approach to simultaneously study dynamical processes in individual ommatidia of the butterfly eyes. A key element in the presented method is the Voronoi diagram. This mathematical tool defines cells, each of which is an assembly of points closest to a certain lattice point. A Voronoi cell is equivalent to the Wigner–Seitz primitive cell in crystallography, which is easily recognized in the cross-section of a compound eye's facet lens (Stavenga, 1979). Eye shine images obtained at the level of the corneal facet lenses therefore can be analyzed straightforwardly with Voronoi diagrams. A morphological image processing (MIP) algorithm (Michielsen and De Raedt, 2001) is used to discriminate the individual facets. The centers of the facets are used to construct a Voronoi diagram, yielding the 'natural' hexagonal topology

* Corresponding author. Tel.: +31-50-3634732; fax: +31-50-3634740.
E-mail address: vanhoutte@phys.rug.nl (K.J.A. Vanhoutte).

0165-0270/$ – see front matter © 2003 Elsevier B.V. All rights reserved.
doi:10.1016/j.jneumeth.2003.08.011

of the original facet lattice. The diagram, superimposed on the image of the corneal facets can then be used to derive information from the underlying ommatidia, e.g. the spatial dimensions of the facet lattice, reflection intensities and spectral characteristics. We provide two examples. First, we show the effect of bleaching the green visual pigment in the homogeneous eye of the nymphalid *Polygonia c-album*. Second, we study the intensity range of pupil activation in green and red-reflecting ommatidia in the heterogeneous eye of the satyrine butterfly *Pararge aegeria*. These examples demonstrate that the developed technique may be a powerful tool to characterize the heterogeneity of butterfly eyes.

2. Materials and methods

2.1. Recording single facet reflections with a digital camera

In our first case study, we have studied the ommatidial reflection after bleaching. The green rhodopsins of butterflies have a peak-absorption typically around 530 nm. Upon photon absorption, the rhodopsin converts into a blue-absorbing metarhodopsin, which is rapidly degraded, resulting in a decreasing absorption called bleaching. Bleaching can be achieved in vivo with a protocol based on repetitive red light flashes (Bernard, 1979). Recently, we investigated the photochemistry in the eye of a nymphalid butterfly, *Polygonia c-album* (Vanhoutte, 2003). The eye shine of this butterfly species suggests that it has an exceptional homogeneous retina (Stavenga, 2002a). To demonstrate the possibility of selective bleaching and to investigate the ommatidial homogeneity we applied the bleaching protocol to a confined eye region. We illuminated the butterfly eye with intense light provided by a Xenon 150 W lamp of a microspectrophotometric set-up, using a microscope objective with a small numerical aperture (4×, NA 0.1, Spindler and Hoyer). Because of the limited field of view of the ommatidia, bleaching of the green visual pigment occurred only locally, i.e. in those ommatidia that had their visual field within the aperture of the illuminating objective. After bleaching, we immediately transferred the animal to a special, wide field microspectrophotometric set-up (Stavenga, 2002b), equipped with an objective with a larger numerical aperture (10×, NA 0.3, Zeiss). A halogen lamp served as the light source. Photographs taken with a digital camera (Kodak, DC120) at the level of the corneal facet lenses were converted in Paint Shop Pro 6 from the standard Kodak format to compressed JPG format with a resolution of 640 × 480 pixels. The image was further cropped to the region of interest for further processing (Section 2.2).

In addition to visual pigment bleaching in the homogeneous eye of *Polygonia c-album*, pupil activation in the eye of the satyrine *Pararge aegeria* was analyzed, specifically in the ventral eye region where the ommatidia are heterogeneous. Two classes of ommatidia, reflecting in the green and red, respectively, stand out (Stavenga, 2002a). Illumination of a dark-adapted (DA) butterfly eye with a bright light source activates the pupil mechanism, i.e. the assembly of pigment granules in the photoreceptors. The granules are driven towards the rhabdom and there reduce the light flux by absorbing light from the boundary wave. The applied procedure was as follows. First, the eye was illuminated for a prolonged period (1 min) with monochromatic light (494 nm) of variable intensity. Five light intensities covering the dynamic range of pupil activation, i.e. about 2 log units, were applied. Immediately after terminating this adapting illumination, a test beam provided by a halogen lamp was delivered to the eye, and the created eye shine was photographed at the corneal level with the digital camera.

2.2. Image analysis

For many industrial, medical and scientific applications, it is well known that some form of digital image processing is necessary before attempting to make measurements of the features in the image. A huge number of different processing steps and methods are available (see for example, Russ, 1995). The type of measurements that will be performed on the images is an important factor in making a selection of the most appropriate processing steps. A quantitative analysis of eye shine images requires the identification of objects (i.e. facets) in the image. Morphological image processing is well suited for this purpose.

MIP uses operations that retain the geometric and topological content of the image (Giardina and Dougherty, 1988; Michielsen and De Raedt, 2001; Russ, 1995). A key concept in MIP is the structuring element or template. A template is a predetermined geometrical structure, hence also an image, such as a square, a disc or a star of a certain size. In essence, MIP is the study of how such a template (or several templates) fits into an image (Giardina and Dougherty, 1988; Michielsen and De Raedt, 2001). A template represents the reviewer's a priori knowledge or expectation about the morphological content of an image.

Two basic MIP operations, used in combination with a template, are the dilation and erosion of an image. Dilation inflates objects in an image, while erosion shrinks objects. These basic morphological operations can be used to construct other, more complicated filtering operations. Two such operations are open and close. Open generally rounds corners from the inside of the objects. Close, on the other hand, smoothens from the outside and removes objects that do not fit the template.

MIP on the eye shine images is performed using the morphological image analysis tool Minko2D (developed by Michielsen et al.). The software makes use of a script language in which the order and frequency of various MIP operations (Michielsen and De Raedt, 2001) can be specified. The first operation in the script transforms the colored (RGB) eye shine image to a gray-scale image. For this transformation the R, G and B channels can be used all

together or separately. In order to identify all facets, the three channels are used simultaneously in the transformation. The fluctuations in gray value within what our eyes would consider being one facet can be rather large. This 'artifact' can be removed from the image by means of open and contrast enhancement operations, using as a template a square or a star. The star is a discretized representation of a disc. The size of the template reflects our rough guess about the size of the objects. Then we map the gray-scale image onto a black-and-white picture (Michielsen and De Raedt, 2001; Russ, 1995). The final step consists of removing some minor artifacts of the size of one pixel by means of an open operation. The end result is a black-and-white image showing rounded structures representing the facets. Minko2D also computes the centers of gravity of these structures. These points represent the so-called facet lattice.

Visual comparison of the original eye shine image and the resulting black-and-white image often shows that not all facets are identified correctly; sometimes facets are grouped and others are missing. This results in defects in the facet lattice. We correct for these defects by taking into account that the facet lattice is a somewhat distorted triangular lattice.

Fig. 1 shows a perfect triangular facet lattice, where each center point is the intersection of three crystallographic directions. In order to find all correct lattice points, it is sufficient to group the facet centers according to two crystallographic directions. The applied procedure works as follows. We collect a fixed number of neighbors for each center point and order them according to their distance to the center point. We average all nearest neighbor distances. The resulting distance gives a rough estimate of the lattice parameter a (Fig. 1). Defects in the lattice can be detected by computing the coordination number C for each lattice point. The coordination number gives the number of nearest neighbors of a lattice point (Ashcroft and Mermin, 1976). In butterfly eye shine images, even if we do not take into account the grouped or missing facets, the facet centers do not form a perfect triangular lattice. Therefore we take the distance $D = 3a/2$ instead of $D = a$ to compute C. In a perfect infinite triangular lattice all points have $C = 6$ (Fig. 1). So-called 'defect points' and points at the boundaries have $C \neq 6$. To group the centers, we first choose a perfect lattice point, i.e. with $C = 6$, and draw lines connecting its nearest neighbors. Then we start from this neighbor and look for the next point in the same crystallographic direction and again draw a line. If no neighbor is found, we start all over with a non-used perfect lattice point and look for its neighbors in the same crystallographic direction as before. At the end of this process, we have groups of points connected by line pieces in one crystallographic direction. In the ideal case, the points are connected by a set of 'parallel lines'. Note that some line pieces that can be seen as belonging to the same 'line' may not be connected. A second group of 'lines', in another crystallographic direction, is created using the same method as described above. At the end of this process, we connect disconnected line pieces, if any, that belong to one single 'line'. We then have two sets of 'parallel lines'. Through each 'line' we fit a second-order polynomial. The intersection of the fitted curves gives a new set of points, which can be considered to represent the facet lattice of the butterfly eye. Finally, we use this new set of points to create a Voronoi diagram. Construction of the Voronoi cells, corresponding to the eye facets, allows the optical characterization of the facets. For each Voronoi cell, we may compute the geometric properties (area, radius), the intensity distribution (average intensities, mode patterns) and the spectral information (color).

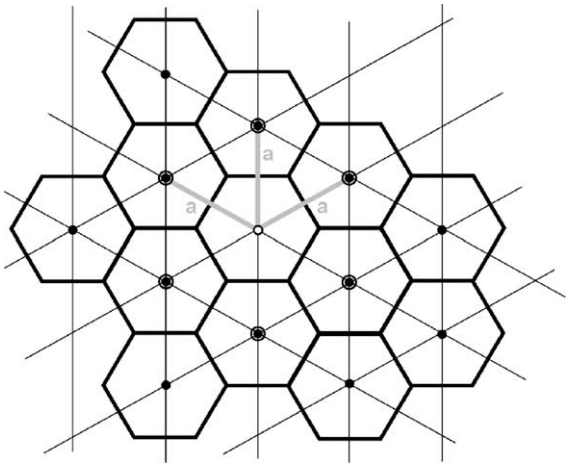

Fig. 1. A perfect triangular facet lattice represented by the dots, with lattice parameter a. The crystallographic directions are indicated by thin black lines and the boundaries of the hexagonal facets by thick black lines. The central lattice point represented by the open circle has six nearest neighbors (points represented by the dots within a circle) and hence has coordination number $C = 6$.

3. Results

3.1. Bleaching green visual pigment in a homogeneous butterfly eye

The eye shine of the comma, *Polygonia c-album*, can be observed at the level of the corneal facet lenses with a large aperture objective. After it has been effectively bleached via a small aperture objective, bright yellow facets in a central region, surrounded by red facets with lower reflectance (Fig. 2), are observed. Decomposition of the original RGB pixel image into its red, green and blue channels shows that the differences in ommatidial reflectance are very minor in the red (R), quite distinct in the green (G) and rather minor in the blue (B) channel, the latter being due to the low blue signal (Fig. 3).

We have used the Minko2D software to identify as many facets as possible in the colored (RGB) eye shine image. We followed the procedure as described in Section 2.2. More details about the procedure are given in Fig. 4. We first transformed the colored image to a gray-scale image using the

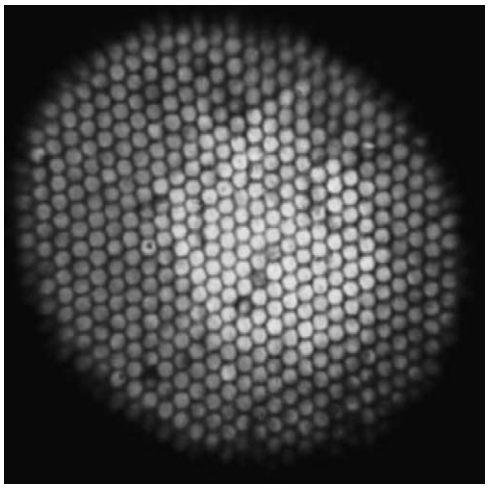

Fig. 2. Overview picture of colorful reflections obtained by epi-illumination microscopy on the eye of the butterfly *Polygonia c-album*. Before bleaching all ommatidia reflect predominantly orange–red light. After applying a bleaching protocol, the central ommatidia reflect yellow due to the depletion of green-absorbing visual pigment.

R, G and B channels simultaneously (Fig. 4A). The maximum of the R, G and B values of a pixel in the original image is taken for the gray-scale value of the corresponding pixel in the gray-scale image. We then applied several open and contrast enhancement operations (Michielsen and De Raedt, 2001), both using as a template a star with a radius of 4 pixels, i.e. containing 49 pixels. Fig. 4B shows the result after the application of one open and one contrast enhancement operation. To further enhance the contrast, we reduced the number of different gray-scale values to 10 and rescaled them afterwards (Fig. 4C). We then mapped the gray-scale image on a black-and-white picture using a threshold of 160. This operation makes all pixels with a value larger than the threshold of 160 white and all others black (intensities or gray values range between 0 and 255). Finally, we removed some small artifacts in the black-and-white image using an open operation with a square of radius 1 (i.e. a square of 3×3 pixels) as template. This operation disconnects facets that are connected by a few pixels only. The whole operation results in a black-and-white image containing 446 objects (Figs. 4D and 5A).

Visual inspection immediately revealed that, as expected, some facets were grouped and others were missing. This gave rise to defects in the facet lattice. They were corrected using the procedure described in Section 2.2. Fig. 5B shows groups of 'lines', connecting the facet centers, in two crystallographic directions (black lines) and the fitted second-order polynomials (gray lines). The black and gray lines largely overlap. The intersections of the fitted curves (gray lines) define the final facet centers. These points were used to construct the Voronoi diagram. The hexagonal Voronoi cells correspond to the original facet lenses (Fig. 6).

Mapping the Voronoi diagram on the images containing only the R, G and B channels of the original RGB picture allowed us to compute the amplitudes of the R, G and B reflections per ommatidium (Fig. 6). We separately summed the R, G and B values of all pixels within a Voronoi cell and normalized to the respective maximal values of all facets. For plotting purposes, we finally normalized all values to numbers between 0 and 99. An example for the green channel of the original eye shine image is shown in Fig. 6, with final values given in each facet.

Peripheral Voronoi cells with an incorrect shape were removed, leaving 340 facets for further analysis (Fig. 7). We chose an intermediate threshold criterion ($G = 43$) to distinguish between bleached and unbleached ommatidia. The criterion was chosen to maximize the inclusion of bleached ommatidia, based on visual inspection. Most green reflection values of the unbleached facets, as given in each cell (Fig. 7A), were well below 40, while most values of the bleached population exceeded the level of 60 (Fig. 7B). The amplitude in both populations, plotted in Fig. 8, shows a rather broad distribution, indicating that the ommatidial reflectance is far from constant, neither in the unbleached nor in the bleached state.

3.2. Pupil activation in a heterogeneous butterfly eye

We have also applied the Voronoi procedure to study the pupil working range in the satyrine butterfly *Pararge*

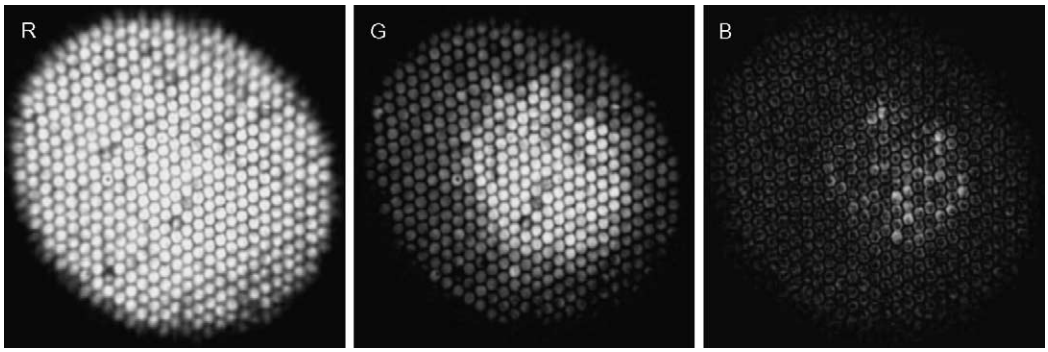

Fig. 3. The image is decomposed into RGB pixel intensity values, clearly showing an increased green (G) reflection in the intensely illuminated (bleached) facets.

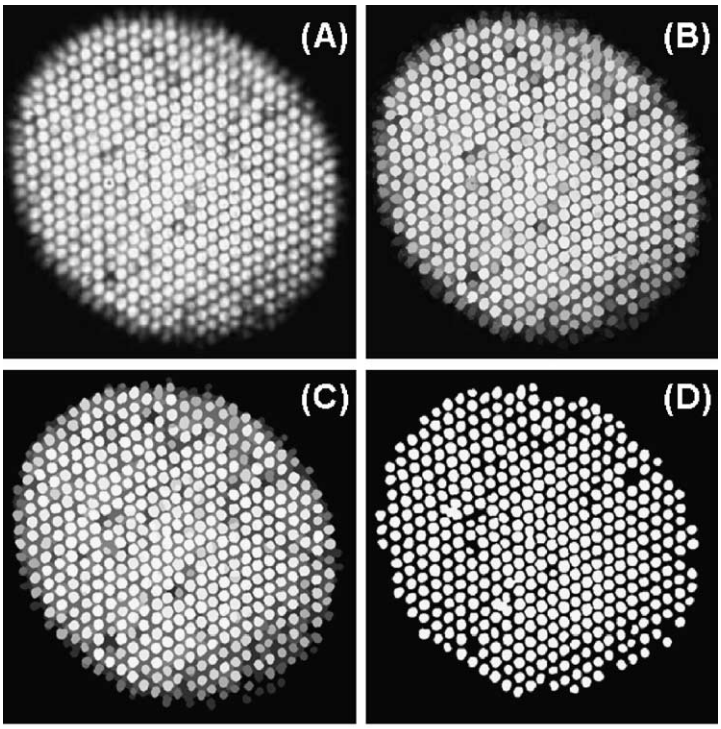


```
RGB_INTENSITY_TO_GRAY                                   (A)

DEFINE_THRESHOLD  number 0 value 160
DEFINE_TEMPLATE number 0 white star of radius 4
DEFINE_TEMPLATE number 1 white square of radius 1

OPEN_GRAY with template number 0                        } (B)
ENHANCE_CONTRAST with template number 0
OPEN_GRAY with template number 0                        } (C)
ENHANCE_CONTRAST with template number 0
OPEN_GRAY with template number 0
GRAY_LEVELS 10
RESCALE_GRAY

GRAY_TO_BLACK_AND_WHITE  with threshold number 0        } (D)
OPEN_BLACK_AND_WHITE with template number 1
```

Fig. 4. Pseudocode of Minko2D software used to detect as many facets as possible in the colored image. Images A, B, C and D show the intermediate results.

aegeria. We investigated pupil activation in individual ommatidia by quantifying the reflection at the corneal level, with the question whether there is a difference in the pupil activation range between red and green reflecting ommatidia. The reflection of the ommatidia is maximal in a dark-adapted eye, and adaptation to increasing light intensities results in a reduced reflection (Fig. 9, inverted gray images 1–5). For the estimation of the pupil activation curves of the red and green reflecting ommatidia, we first constructed a Voronoi diagram, following the procedure described in Section 2.2, based on the dark-adapted picture. The reflection intensities of the Voronoi cells (29 red and 96 green reflecting facets) were then averaged and normalized with the reflection intensities of the DA image. For each facet the normalized reflection data for the five illumination intensities was subsequently fitted with the sigmoid function:

$$y = \{1 + \exp[s(P - P_{50})]\}^{-1}$$

where P is the decadic logarithm of I with I the photon flux; s a slope constant; P_{50} the 50% pupil activation threshold. Finally, for both red and green facets a mean pupil activation curve, the averaged sigmoid function, was calculated, together with the standard deviation for the five illumination intensities. A histogram of the flux intensities that elicit 50% pupil activation (P_{50}) shows that the range of the activation threshold criterion for all facets is restricted to 0.5 log units.

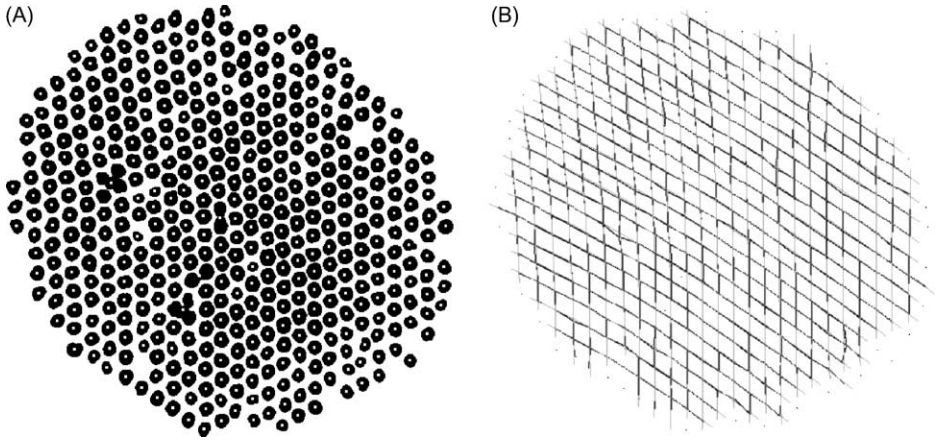

Fig. 5. Image processing (in Minko2D) to determine facet lens center points. (A) Facet centers detected by a MIP algorithm are superimposed on the binary image. Clearly the procedure results in missing facets or connected facets. (B) Lines through the center points, which are correctly identified, are drawn in black. The intersection points of fitted second-degree polynomials (gray lines) define the new coordinates.

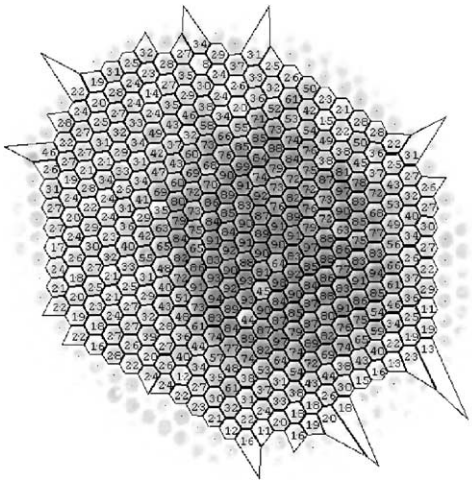

Fig. 6. Construction of the Voronoi diagram and quantification of the reflection within cells. The Voronoi diagram is constructed from the facet center coordinates after image processing (see Fig. 5). The diagram is plotted on the inverted gray image of the green intensity values. The RGB reflection values of all points within a cell then are integrated and normalized to the maximal value of all facets, yielding normalized ommatidial reflection values with two digits (maximum 99). The individual values of the G channel are plotted in the center of the individual facets.

The distributions of both populations partially overlap and reflect a similar pupil working range in both red and green reflecting facets. Statistically (one sided *t*-test, $\alpha = 0.05$) the mean P_{50} (12.6 log units) of the green facets is lower than the mean P_{50} (12.9 log units) of the red facets.

4. Discussion

4.1. A new method to quantify single facet reflections

The Voronoi algorithm is widely applied in mesh generation problems and partitions space around geometric objects into cells, each of which consists of points closer to one particular object than to all other objects (Aurenhammer, 1991; Okabe et al., 1992). Here the diagram defines interconnected hexagonal areas fully overlapping with the facet lenses of butterfly eyes.

The eye shine of a large number of ommatidia can be photographed with a new telemicroscopic set-up (Stavenga, 2002a,b). The procedure described in the present paper allows the analysis of the reflected light emerging from individual ommatidia, owing to their regular ordering in a two-dimensional lattice. First, we used a MIP tool to detect the individual facet centers (Michielsen and De Raedt, 2001). Next, after the necessary corrections (see Section 2.2) the assembly of facet centers was fitted to a two-dimensional lattice. The lattice is constructed here with second-order polygonal lines fitted through the facet centers, to take into account the slight gradients in the eye. Finally, the coordinates of the lattice points were used to create a Voronoi diagram.

4.2. Simultaneous analysis of individual ommatidia

We have demonstrated the ‘Voronoi procedure’ in two preliminary case studies. First, we investigated bleached ommatidia in the butterfly eye. After superimposing a Voronoi diagram, we quantified the averaged RGB intensity values (Figs. 6–8) from individual facets. Bleached and unbleached ommatidia are clearly distinguished in the green intensity values, reflecting the decreased absorption in bleached ommatidia, because of depletion of green absorbing visual pigment (Bernard, 1979; Vanhoutte, 2003). It thus appeared that the reflection of the individual ommatidia in both populations is quite variable (Fig. 8). Sources of variation may constitute slightly different mode radiation patterns, related to differences in rhabdom size, differences in visual pigment densities or the intrinsic variation of the underlying tapeta

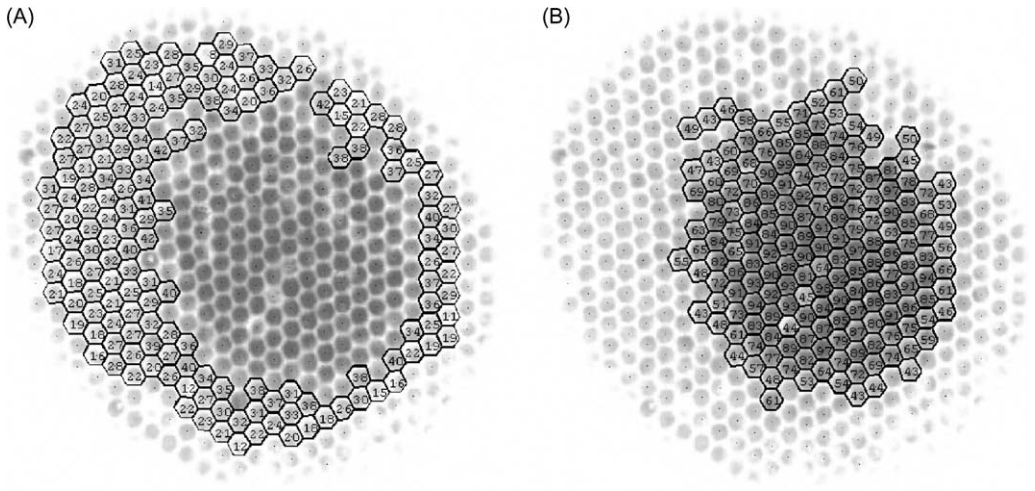

Fig. 7. Selection of bleached ommatidia based on the calculated integrated reflection values of Fig. 6. An appropriate threshold criterion was chosen ($G = 43$) to distinguish between bleached and unbleached ommatidia. (A) Most unbleached facets have intensity values well below the criterion level 43. (B) All bleached facets coincide with green intensity values = 43 (see also Fig. 8).

and their reflectance spectra (unpublished data). Inhomogeneous illumination and the curvature of the eye may add artificial noise to the recordings. Further research is required to clarify this point. The result may put into question the reliability of the butterfly eye as an absolute light detector, but it will be more intriguing to analyze whether the uncovered optical variability affects contrast sensitivity, the more probable aim of an eye.

As a second example, we investigated the pupil working range in the ventral eye region of the satyrine butterfly *Pararge aegeria*. A green–red ommatidial eye shine is observed here, similar to the eye shine in the ventral half of the eye of the satyrine butterfly *Bicyclus anynana* (Stavenga, 2002b). In contrast to previous reflectometric recordings in butterfly eyes at the level of the deep pseudopupil (Järemo Jonson et al., 1998), we here analyzed images of the corneal reflection after different illumination intensities. The integrated signal at the deep pseudopupil neglects the heterogeneous properties of the individual ommatidia, which may cause serious errors, especially in the ventral eye region.

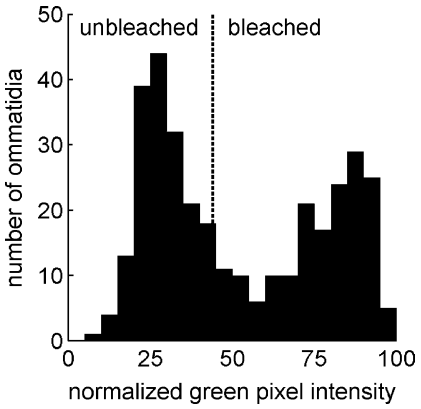

Fig. 8. Intensity distribution histogram of bleached and unbleached single facet values for the green pixel intensity. The threshold criterion ($G = 43$) to distinguish between bleached and unbleached ommatidia is indicated with a dashed line. The mean averaged green pixel intensity is 76 for the bleached facets and 28 for the unbleached facets (see Table 1).

We have found an apparent dynamic range of approximately 2 log units for the pupil mechanism (Fig. 9A), corroborating previous studies (Järemo Jonson et al., 1998; Stavenga, 1979). Interestingly, the pupil range of the red and green reflecting ommatidia is rather similar. The ommatidia with green facets seem to have a slightly lower light threshold than the ommatidia with red facets for blue–green light (494 nm). Possibly this is related to the short-wavelength absorbing, red screening pigment, which presumably borders the rhabdom in red-reflecting facets and shifts the light sensitivity towards longer wavelengths (cf. Stavenga, 2002b). However, the 50% activation criterion values vary over 0.5 log units in both the green and red-reflecting ommatidia (Fig. 9B). In addition to the intrinsic sources of variability in ommatidial reflectance mentioned above, likely a variable density of pupil granules along the rhabdom also contributes to the observed variation. Further detailed measurements are necessary to substantiate this point.

4.3. Perspectives

Beautiful colored reflections over a large eye area can be digitally recorded in a specialized optical set-up (Stavenga,

Table 1
The mean reflection value ± S.D. of the pixel intensities (RGB) averaged over a single facet area

All facets ($n = 340$)	R	G	B
Unbleached ($n = 172$)	52 ± 5	28 ± 8	17 ± 3
Bleached ($n = 168$)	51 ± 3	76 ± 14	32 ± 16

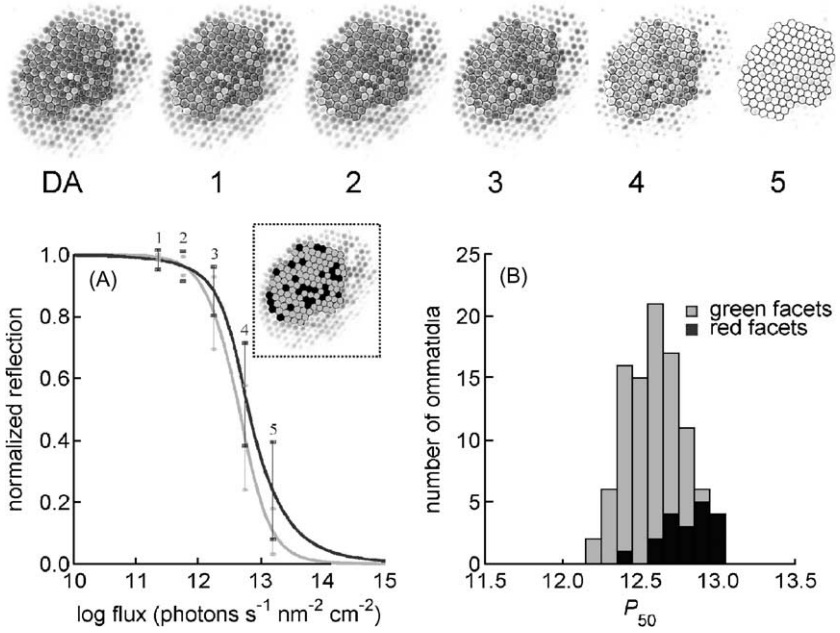

Fig. 9. Pupil activation in the ventral area of the satyrine *Pararge aegeria*. Top panel: Immediately after prolonged illumination with monochromatic light (494 nm) the corneal reflection is recorded with a digital camera (shown here as inverted gray images 1–5). The illumination intensity was varied with five density filter combinations covering the dynamic range of pupil activation. Illumination with weak light does not trigger pupil migration as the reflection is not different from the control image in the dark-adapted state (compare picture 1–2 and DA). (A) The pupil is gradually activated while increasing the intensity, and finally results in virtually complete 'pupil closure' (picture 5). We calculated the mean pupil activation curve for 29 red-reflecting ommatidia (black line) and 96 green reflecting ommatidia (gray line). The mean curve, together with the standard deviation at the five illumination intensities, was calculated after fitting sigmoid functions through the normalized reflection intensities. Therefore, a Voronoi diagram was calculated based on the DA picture. The location of the red and green facets is indicated by black and gray colored Voronoi cells, respectively (inset). The illumination intensity is expressed as the photon flux at the focal plane of the objective. (B) Histogram of the flux intensities that elicit 50% pupil activation (P_{50}). This activation threshold criterion holds for all facets within 0.5 log units. The distributions of both populations partially overlap. Statistically (one sided *t*-test, $\alpha = 0.05$) the mean P_{50} of the green facets (12.6 log units) is lower than the mean P_{50} of the red facets (12.9 log units).

2002b). The challenge is now to set-up an automated fast analysis procedure of reflection data from the eyes of butterflies to quantify the spatial properties and to unmask the optical properties of the underlying light regulating machinery. Research topics of immediate interest include the study of pupil activation, visual pigment kinetics, spatial resolution, heterogeneity in the ventral area and the development of the eye structure. We have started to explore the spectral sensitivity of the pupil mechanism by pupil activation with selective monochromatic illuminations of variable intensity (unpublished results). The automated analysis will enable a comparative survey of the eyes of different butterfly species.

Acknowledgements

We thank H. Leertouwer and B. Pijpker for invaluable technical assistance. K.F.L.M. acknowledges useful discussions with Prof. H. De Raedt.

References

Arikawa K, Stavenga DG. Random array of colour filters in the eyes of butterflies. J Exp Biol 1997;200:2501–6.

Ashcroft NW, Mermin D. Solid state physics. Philadelphia: Saunders; 1976.

Aurenhammer F. Voronoi diagrams: a survey of a fundamental geometric data structure. ACM Comput Surveys 1991;23:345–405.

Bernard GD. Bleaching of rhabdoms in eyes of intact butterflies. Science 1979;219:69–71.

Bernard GD, Remington CL. Color vision in *Lycaena* butterflies: spectral tuning of receptor arrays in relation to behavioral ecology. Proc Natl Acad Sci USA 1991;88:2783–7.

Franceschini N, Kirschfeld K. Les phénomènes de pseudopupille dans l'oeil composé de *Drosophila*. Kybernetik 1971;9:159–82.

Giardina CR, Dougherty ER. Morphological methods in image and signal processing. Englewood Cliffs: Prentice-Hall; 1988.

Järemo Jonson AC, Land MF, Osorio DC, Nilsson DE. Relationships between pupil working range and habitat luminance in flies and butterflies. J Comp Physiol A 1998;182:1–9.

Michielsen K, De Raedt H. Integral-geometry morphological image analysis. Phys Rep 2001;347:461–538.

Miller WH, Bernard GD. Butterfly glow. J Ultrastruct Res 1968;24:286–94.

Okabe A, Boots B, Sugihara K. Spatial tesselations: concepts and applications of Voronoi diagrams. New York: Wiley; 1992.

Russ JC. The image processing handbook. Boca Raton, FL: CRC Press; 1995.

Stavenga DG. Visual adaptation in butterflies. Nature 1975;254:435–7.

Stavenga DG. Colour in insect eyes. J Comp Physiol A 2002a;188:337–48.

Stavenga DG. Reflections on colourful butterfly eyes. J Exp Biol 2002b;205:1077–85.

Stavenga DG, Numan JAJ, Tinbergen J, Kuiper JW. Insect pupil mechanisms. II. Pigment migration in retinula cells of butterflies. J Comp Physiol A 1977;113:73–93.

Stavenga DG. Pseudopupils of compound eyes. In: Autrum H, editor. Handbook of sensory physiology, vol. VII/6A. Berlin: Springer; 1979. p. 357–439.

Vanhoutte KJA. Butterfly visual pigments: molecular cloning and optical reflections. Thesis. Rijksuniversiteit Groningen; 2003.